Rare-earth dependence of photoinduced chain-oxygen ordering in $R\mathrm{Ba_2Cu_3O_{7-x}}$ ($x \approx 0.3$) investigated by Raman scattering

S. Bahrs, A. R. Goñi, and C. Thomsen
Institut für Festkörperphysik, Technische Universität Berlin, Hardenbergstrasse 36, 10623 Berlin, Germany

B. Maiorov, G. Nieva, and A. Fainstein
Centro Atómico Bariloche, Comisión Nacional de Energía Atómica, 8400 San Carlos de Bariloche, Río Negro, Argentina

(Received 17 August 2001; published 19 December 2001)

We investigated a set of oxygen-deficient $R\mathrm{Ba_2Cu_3O_{7-x}}$ ($x \approx 0.3$) ceramic samples with Raman spectroscopy under resonant conditions for the defect-induced Cu-O chain related modes at 230 and 600 $\mathrm{cm^{-1}}$. Emphasis was laid on the frequency and intensity of the modes for different rare-earth atoms, and especially on their dependence under illumination. The modes display photoinduced bleaching for all R, including the nonsuperconducting $R=\mathrm{Pr}$. The dynamics of their bleaching following a temperature quench indicates similar complex relaxation processes for all samples. A simple stretched exponential with a common $\beta = 0.36 \pm 0.04$ and a distribution of time constants ranging from 50 to 1400 s describes our data well. We discuss our results in connection to photoinduced chain-oxygen ordering in oxygen-deficient superconductors.

DOI: 10.1103/PhysRevB.65.024522 PACS number(s): 78.30.-j, 74.72.Bk, 64.60.Cn, 73.50.Pz

I. INTRODUCTION

The oxygen content determines the conduction properties in the $R\mathrm{Ba_2Cu_3O_{7-x}}$ family of high-T_c superconductors, yielding a superconducting transition temperature $T_c = 90\,\mathrm{K}$ for the fully oxygenated orthorhombic phase, and $T_c \approx 60\,\mathrm{K}$ for an oxygen-deficient phase (for $R=\mathrm{Y}$, $x \approx 0.4$). For lower oxygen contents the material becomes tetragonal and insulating (in $R=\mathrm{Y}$, $x>0.6$). The oxygen defects in nonstoichiometric material occur on the chain-oxygen site, interrupting the Cu-O chains of the fully oxygenated material. On a macroscopic scale and for specific values of x, the oxygen defects may be ordered in particular ways as determined, e.g., from neutron scattering.[1,2] Apart from the oxygen content, the distribution of defects influences the conduction properties of the material. The ordering of the oxygen atoms changes the average valence of the Cu atoms, which in turn results in an increased doping of the superconducting $\mathrm{CuO_2}$ planes.[3] A large experimental and theoretical effort has been devoted to understanding the conduction and structural properties of the differently ordered phases.[1–5]

Oxygen-deficient samples were also found to show slightly increased conductivity and T_c under illumination. The persistent photoconductivity (PPC) effect and the photoinduced enhancement of superconductivity (PES) is stable after illumination at temperatures lower than 200 K, but the original state recovers with annealing at higher temperatures.[6,7] The dynamics of the photoinduced effects can be described by a stretched exponential,[4] the so-called Kohlrausch law for relaxation processes in disordered systems. The properties and dynamics of these PPC effects resemble those of a number of defect-induced Raman modes occurring only in oxygen-deficient materials. These modes, which were assigned to the Cu-O chains,[8] lose intensity under illumination and recover with annealing in the dark.[9] The normally weak modes can be studied under resonant excitation at $\lambda_{\mathrm{exc}} = 568\,\mathrm{nm}$ and behave similarly to PPC and PES with respect to the bleaching.[9–12]

Considering the similarities in the dynamics, it is tempting to connect the photoinduced effects on the electrical properties to those on the defect-induced Raman vibrations. The origin of these modes has been discussed by a number of groups. They explain the defect modes in terms of Cu-O chain vibrations, which are Raman forbidden for the infinite chains of the perfect orthorhombic crystal, but which become active due to the disorder of oxygen in the chains.[13] Altering the order by light-activated diffusion of chain-oxygen atoms, which increases the length of chain fragments, would result in a decreased defect density and an increased doping of the conduction planes, which is compatible with both transport and Raman-scattering observations.[10–12,14–16] However, in spite of the assignment of the vibrational modes to the oxygen chains several points remain under discussion: First, the mechanism of activation of the modes and second, whether the dynamics of oxygen diffusion for an initial state at a given temperature (or quench) and a final state after illumination can account for its time dependence.

So far, most of the published work has been performed on $\mathrm{YBa_2Cu_3O_{7-x}}$ with a few reports confirming the effects of PPC and photobleaching of the Raman signals also in samples with a different rare-earth atom, $R=\mathrm{Gd}$ (e.g., Ref. 10). Within the proposed oxygen diffusion model, the size of the crystallographic unit cell, which directly depends on the size of the rare-earth atom, should sensitively determine the activation energy for oxygen diffusion. Apart from the increase in size, larger rare-earth atoms in the compound form more tetragonal structures since the a axis, which is shorter in fully oxygenated material, increases more with the ionic radius than does the b axis.[17]

In this paper we studied the frequency and photoexcitation-time dependence of the defect-induced Raman modes in a set of samples with different R ($R=\mathrm{Y}$, Er, Eu, Sm, Nd, La, and Pr), also including $R=\mathrm{Pr}$, the only nonsuperconducting variation of $R\mathrm{Ba_2Cu_3O_{7-x}}$. Our study aims at determining the parameters important for the photoexcitation phenomena. We evaluated the photobleaching data using a stretched exponential and analyzed the bleaching parameters

as a function of the ionic radius of the rare-earth atom. We find good agreement of our results with the model of oxygen ordering and diffusion in the planes of the oxygen chains.

II. EXPERIMENTAL DETAILS

Our samples of ceramic $R\mathrm{Ba_2Cu_3O_{7-x}}$ were prepared by a solid-state reaction of stoichiometrically mixed powders as described in Ref. 18. The final sintering temperatures varied from 950 °C to 970 °C in flowing oxygen for all R with the exception of $R=\mathrm{La}$, which was sintered at 970 °C in N_2, followed by annealing in oxygen. The oxygen content reduction was performed at 507 °C in an oxygen atmosphere of 14.5 mbar followed by a controlled cooling process, which corresponds to $x=0.3$ for $R=\mathrm{Y}$.[19] The same procedure was followed for all ceramics of the R123 series, since the O_2 pressure-temperature diagrams are very similar for $R=\mathrm{Gd}$ (Ref. 20), Y, Pr, Nd, and La,[21] except for La near maximum oxygen stoichiometry. Nevertheless, for our La sample we have measured a T_c value of 94(1) and 10(3) K before and after oxygen reduction, respectively. The latter is in good agreement with literature data for an oxygen deficiency of $x=0.3$.[22] The samples were kept at room temperature in the dark for several weeks and then quenched from 293 to 80 K within 10 min using an Oxford cryostat. All bleaching measurements were recorded at 80 K on a previously unilluminated spot of the sample using a triple Dilor spectrometer in backscattering geometry with a nitrogen-cooled charge-coupled device detector. For excitation the 568-nm line (6 mW) of an Ar^+-Kr^+ laser was focused on a spot of about 100 μm in diameter. The laser light served as excitation as well as for bleaching of the samples. The bleaching was observed by sequentially taking spectra with accumulation times of 5 and 10 min for a total illumination period of two hours.

III. RESULTS AND DISCUSSION

The Raman spectra of all samples are shown in Fig. 1: The spectra are arranged by order of the ionic radius of the rare-earth atom (and hence the tetragonality of the unit cell) with the smallest, Er, at the top. The allowed Raman modes[23] at about 330 $\mathrm{cm^{-1}}$ (B_{1g}-like in D_{4h}), and at 460 and 500 $\mathrm{cm^{-1}}$ (both A_{1g}-like) are visible in all spectra except for those of $R=\mathrm{Sm}$ and Nd, where the 330 $\mathrm{cm^{-1}}$ mode is very weak (see position markers). The dominant features, however, are the defect-related structures at 230 and 600 $\mathrm{cm^{-1}}$. The peaks around 230 $\mathrm{cm^{-1}}$ are clearly present for all R including Pr. They gain in intensity for smaller ionic radii, which can be seen on an absolute scale as well as in comparison to the intensity of the B_{1g}-like Raman-allowed mode (see discussion of Fig. 3 below). The structures around 600 $\mathrm{cm^{-1}}$ are resonant as well, though weaker. In contrast to the low-frequency group, they show no apparent systematic dependence of the intensity on the ionic radius of R. For $R=\mathrm{Pr}$ the high-frequency peaks are missing completely. Apart from the aspect of overall intensity, the spectra of the more orthorhombic material are more complex than the tetragonal ones. Whereas only peaks at 225, 263, and 598 $\mathrm{cm^{-1}}$ can be distinguished in the La spectra, six peaks in two groups around 230 and 600 $\mathrm{cm^{-1}}$ are present for $R=\mathrm{Y}$ (234, 265, 291, 309, 579, and 597 $\mathrm{cm^{-1}}$).

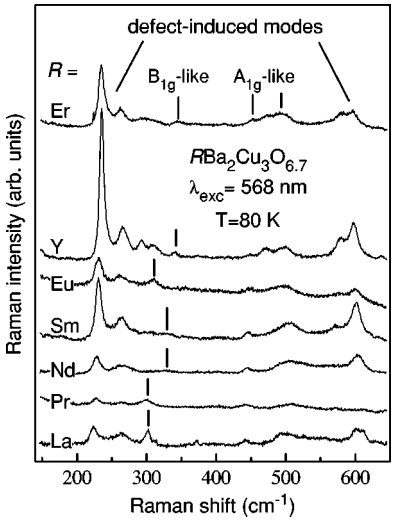

FIG. 1. Raman spectra of ceramic samples of oxygen-deficient $R\mathrm{Ba_2Cu_6O_{6.7}}$ taken at $T=80\,\mathrm{K}$ ($\lambda_{exc}=568\,\mathrm{nm}$). The spectra are offset for clarity, but have the same integration time and scale factor. The defect-induced modes at 230 and 600 $\mathrm{cm^{-1}}$ are not Raman allowed in the fully oxygenated, ideal crystal. In $\mathrm{YBa_2Cu_3O_{6.7}}$ these modes are resonant at this excitation wavelength. The frequencies of all modes depend on the radius of the rare-earth atom as shown in Fig. 2.

An interesting aspect is the frequency shift of the two defect-induced features with ionic radius as shown in Fig. 2. Similarly to the Raman-allowed modes at 330 and 500 $\mathrm{cm^{-1}}$,[24,25] they shift in opposite directions with (-65 ± 8) for the 230 and $(58\pm10)\,\mathrm{cm^{-1}/\AA}$ for the 600-$\mathrm{cm^{-1}}$ peak. These slopes are smaller than those of the 330- and 500-$\mathrm{cm^{-1}}$ modes [(-290 ± 50) and $(119\pm12)\,\mathrm{cm^{-1}/\AA}$, re-

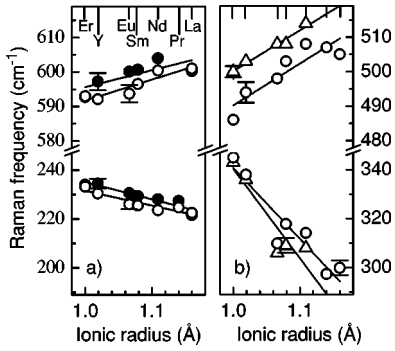

FIG. 2. Frequency of the main defect-induced peaks (a) for the different rare-earth atoms in comparison to that of the Raman-allowed modes around 330 and 500 $\mathrm{cm^{-1}}$ (b). The triangles represent data for fully oxygenated samples taken from Ref. 24. Full symbols correspond to $T=80\,\mathrm{K}$, open ones to room temperature. The frequencies of the allowed modes in the 80-K spectra do not deviate from the room-temperature data significantly and are not shown. The systematic shift with ionic radius of the defect-induced modes is similar to that of the Raman-allowed ones, but is less pronounced.

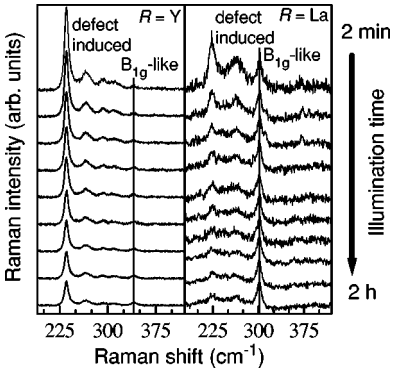

FIG. 3. Sequence of Raman spectra of continuously illuminated $R=$Y and La samples. The frequency interval shown includes a Raman-allowed and a defect-induced mode. The La spectra have been multiplied by a factor of 4. Whereas the Raman-allowed mode remains unperturbed, the intensity of the defect mode decreases under the influence of light in both samples.

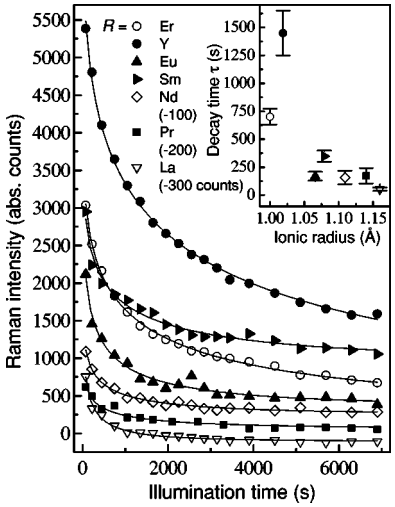

FIG. 4. Intensity of the peak at 230 cm^{-1} over illumination time for ceramic samples of $RBa_2Cu_3O_{6.7}$. For clarity, the lower three curves were offset by the amounts given in the legend. The fits were performed using a stretched exponential law with a common exponent $\beta=0.36\pm0.04$ for all data sets (see Table I). The inset shows the relaxation time τ depicted versus the ionic radius of R.

spectively]. As already mentioned, an increase of the lattice parameters is produced by increasing the rare-earth size.[17] Thus, in principle a softening of the phonon energies could be expected due to a reduction of the force constants. However, substituting a larger atom in the center does not lengthen all bonds in the unit cell uniformly. Instead, the distance between the Cu atom in the chains (Cu1) (Ref. 26) and in the planes (Cu2) decreases, while the separation of the CuO_2 planes increases such that an overall lengthening of the c axis results. This explains the change in force constants for the 330- and the 500-cm^{-1} modes in opposite directions. The former corresponds to an OII-OIII out-of-phase vibration[26] in the planes and softens, whereas the latter is a vibration of the bridging oxygen atom between Cu1 and Cu2 and hardens.

For the defect-induced modes it is less clear why the two modes related to the chain oxygen (OI) shift in opposite directions with an increasing rare-earth radius. An increased unit-cell parameter (b) would lead to an elongation of the Cu1-OI bonds and hence to weaker stretching and bending vibrational frequencies. While the latter is observed for the 230-cm^{-1} vibration in Fig. 2 the high-frequency mode at 600 cm^{-1} does not follow this simple explanation. Its hardening with increasing rare-earth ionic radius, though weak, appears to be linked in a more sophisticated way to that of the dependence of the OIV mode in fully oxygenated $RBa_2Cu_3O_{7-x}$ as shown in Fig. 2(b). The frequencies of the defect modes have been determined at two different temperatures [see Fig. 2(a)]. As expected, they are slightly softer at room temperature than at 80 K (in agreement with the findings of Ref. 27 for $R=$Y).

After discussing the frequencies of the defect-induced modes we now turn to their initial amplitude in the spectra and their dynamics. In Fig. 3 a series of spectra is shown for the $R=$Y and La samples in an expanded frequency interval including the defect at 230 cm^{-1} in Y or 225 cm^{-1} in La and one of the Raman-allowed modes (340 and 300 cm^{-1}, respectively). The first measurement is shown at the top, and the illumination time grows up to two hours down at the bottom. Turning to the La spectra, we find the Raman-allowed mode to keep the same amplitude in all spectra, whereas the defect mode diminishes and finally vanishes in the background. For $R=$Y, the situation is generally the same, but the details differ. The defect mode is much larger to start with; in comparison, the Raman-allowed mode is hardly visible on the same scale. Furthermore, we observe that the whole defect-induced structure decreases in the same way pointing towards a close relation of the various peaks.

There are several possible reasons for the rare-earth dependence of the initial intensity of the defect-induced peak at 230 cm^{-1}: First, all spectra were integrated over the same finite time interval. The effect of photobleaching cannot be separated from that of illumination during spectroscopy. The rare-earth-substituted samples bleach with different rates and hence have different intensities after the initial integration. However, extrapolations of time-dependent measurements to the initial intensities (see Fig. 4, Table I, and a later discussion) still yield different values. Bleaching can therefore only be part of the reason. Second, the intensity of the defect

TABLE I. Fit parameters for a stretched exponential function. We performed a simultaneous fit with a shared (but variable) exponent β for all data sets.

$RBa_2Cu_2O_{6.7}$	Exponent $\beta=0.36\pm0.04$	
R	Initial intensity I_0	Decay constant $\tau(s)$
Er	4400±400	700±70
Y	7400±500	1400±200
Eu	3700±400	170±40
Sm	3400±300	350±50
Nd	1900±300	160±60
Pr	1200±100	170±70
La	2700±300	50±15

modes strongly depends on the exact oxygen content of the sample, as is shown in Ref. 12 for $R=\mathrm{Y}$. The apparent systematics in the initial amplitude could reflect that of oxygen diffusion for different rare-earth atoms during preparation. Third, the resonance profile was determined for a $R=\mathrm{Y}$ sample (maximum at 2.15 eV, width 0.17 eV, see Ref. 11), and the wavelength with the strongest resonance in Y might well be slightly ''out of tune'' for the other rare-earth-substituted compounds, corresponding to a direct dependence of the resonant energy on *R*.

The considerably larger defect-induced modes for $R=\mathrm{Y}$ after two hours are not only due to their larger initial amplitude, but also to a slower decay with time, upon which we will focus now. Figure 4 shows the intensity of the 230-cm^{-1} defect mode versus illumination time for various rare-earth-substituted samples. The origin of the time axis is set to the beginning of the illumination. For all *R* the defect modes decrease substantially with illumination time. The nonsuperconducting compound with $R=\mathrm{Pr}$ does not show exceptional behavior in this respect. We evaluated the data using a stretched exponential function,

$$I(t)=I_0\exp\left(\frac{t}{\tau}\right)^{\beta}+\text{const.}$$

This Kohlrausch law is applied to the relaxation processes in disordered, amorphous, or complex systems such as glasses and highly doped semiconductors[28] and can be traced back theoretically to a distribution of relaxation constants.[29] In this scenario τ is interpreted as a relaxation time similar to those in the usual exponential decay laws, while the exponent β is related to a wide distribution of relaxation times or to the degree and type of disorder.[29] Accordingly, β can be interpreted as an indicator for the disorder in the chain-oxygen pattern, which is believed to be frozen in during the temperature quench.

Since we treated all samples alike in the quenching procedure, a common value of β would be in good agreement with the type of disorder suggested. In fact, fits to the data sets of the individual samples yielded similar values for the exponent, though in some cases ($R=\mathrm{Sm}$, Pr, and La) with high statistical uncertainties. Taking β to be the same for all data sets (but variable) we can fit our results with $\beta=0.36\pm0.04$ and τ and I_0 as given in Table I. The fits are also shown in Fig. 4 and describe the data well. In contrast to the exponent β, the decay constant τ does depend on the rare-earth atom. The values of τ are depicted versus the ionic radius of *R* in the inset to Fig. 4. The bleaching of the modes tends to become faster for larger ionic radii. Within the chain-oxygen ordering model a qualitative explanation could be as follows. With increasing rare-earth radii the basal plane bond lengths (and lattice parameters *a* and *b*) increase, while the orthorhombic distortion caused by the chain oxygens becomes less pronounced.[17] The lengthening of the bonds decreases the activation energy necessary for the diffusion of the oxygen atoms, which speeds up their reorganization within the planes of the chains.

Aligia and Garcés[3] showed that the average valence of the chain Cu atoms changes with the reorganization of O atoms in the chains in oxygen-deficient material. The doping of the CuO_2 planes by the Cu-O chains, in their model, is higher for a mixture of Cu atoms with two and zero neighboring O atoms than it is for an average of one neighboring oxygen atom per Cu atom. Under certain conditions (temperature and oxygen-concentration dependencies), the two possibilities also have different total energy. This corresponds to the different phases with varying oxygen content and temperature. They were investigated by a number of groups in theoretical as well as experimental approaches.[2,5,30] They showed that it is energetically favorable for the oxygen atoms in the chains to not spread stochastically on the sites between Cu atoms, but rather to become organized in patterns. For a deficiency of 0.5, the simplest pattern consists of alternating full and empty chains, a configuration that has been found and named the ortho-II phase. More complicated structures for other oxygen concentrations, like the ortho-III phase or patterns in which the oxygens form regular islands, were also investigated.[2]

In the light of this work, explaining persistent photoconductivity and Raman mode bleaching could run as follows: During the temperature quench, a state of disorder in the distribution of oxygen atoms in the Cu-O chains becomes frozen, when the relaxation times for reaching a new energetically more favorable state grow much longer than the inverse cooling rate. This corresponds well to the results of Nagel *et al.*, who found a glasslike transition in the thermal expansivity of oxygen-deficient material upon cooling at about 280 K.[31] This leaves the system in a disordered state, in which neither the total energy nor the doping level of the superconducting planes is at optimum. The number of defects, that is, open chain ends, are large right after the quench. Illuminating the sample in this state provides the activation energy for the oxygen atoms to change site. We believe that during diffusion the energetically favorable superstructures form, increasing the doping level and the average length of the chains. The dynamics of this process will likely be described as a relaxation in a glass, for which stretched exponential laws have successfully been applied.

An increased conductivity and transition temperature and their time dependencies are the direct consequence of the above-described process. For the bleaching of the observed defect modes reported here, the connection depends on the activation mechanism of the defect-induced modes. A number of models have been discussed in the literature.[12,11,16] The modes could be Γ-point infrared-active modes activated through the symmetry loss in oxygen-deficient material. However, this would not explain the large number of peaks that was observed, e.g., in the $YBa_2Cu_3O_{7-x}$ spectra (Fig. 1). Another possibility is that the modes are activated by a zone folding caused by the formation of various superstructures of the OI oxygen atoms.[12] This, however, should yield shifting numbers and frequencies of peaks for different oxygen contents, opposite to what has been observed so far. Assigning the peaks to Cu_2O monomers and oxygen-chain fragments as in Refs. 10 and 16 can account for a larger number of peaks as well as an unperturbed frequency. But in this case there should be a clear and individual dependence of intensity of each peak on the overall oxygen content, which could not be

confirmed. We therefore argue in favor of a defect-induced Raman visibility of the partial density of states corresponding to the phonon branches of the chains as calculated, e.g., by Kress *et al.*[32] Within this model, the defects (chain ends) make the structures appear in the spectra, and the lengthening of the chains during illumination corresponds to the observed decrease in intensity. This can explain the number of peaks in the spectra and the fact that all additional peaks behave similarly in the bleaching, reflecting a common origin. The systematic development in frequency and complexity of the defect structures for different rare-earth atoms is then connected to the dispersion of the branches, which slightly shift for different rare-earth atoms in place of *R*. This is seen in the frequency dependence of the defect modes in Fig. 2. The increased orthorhombicity accounts for the larger number of modes distinguished for $R=$Er, Y, and Sm.

IV. CONCLUSIONS

In conclusion, we observed defect-induced modes and their bleaching under illumination in a series of samples of oxygen-deficient $R\mathrm{Ba_2Cu_3O_{7-x}}$. The Raman frequencies of the 230- and 600-cm^{-1} modes change rather systematically with the ionic radius of the rare-earth atom. Similar systematics are found for the initial intensity of the 230-cm^{-1} mode but not for the 600-cm^{-1} mode. The dynamics of bleaching of the 230-cm^{-1} peak can be described by a stretched exponential law, yielding a value of $\beta=0.36\pm0.04$ and a rare-earth-dependent relaxation time. We attribute the effect and its dynamics to an ordering of oxygen atoms in the planes of the Cu-O chains and connect it directly to the change of conductivity under illumination. The photoinduced enhanced superconductivity in oxygen-deficient $R\mathrm{Ba_2Cu_3O_{7-x}}$ should thus also depend on the rare-earth atom.

ACKNOWLEDGMENTS

This work was supported by the Deutscher Akademischer Austauschdienst (DAAD) and the Agencia Nacional para la Promoción Científica y Tecnológica of Argentina under the program PROALAR 2000. We acknowledge helpful discussions and assistance from G. Levy and E. Osquiguil.

[1] J. D. Jorgensen, Shiyou Pei, P. Lightfoot, Hao Shi, A. P. Paulikas, and B. W. Veal, Physica C **167**, 571 (1990).
[2] N. H. Andersen, M. von Zimmermann, T. Frello, M. Käll, D. Mønster, P.-A. Lindgård, J. Madsen, T. Niemöller, H. F. Poulsen, O. Schmidt, J. R. Schneider, Th. Wolf, P. Dosanjh, R. Liang, and W. N. Hardy, Physica C **317–318**, 259 (1999).
[3] A. A. Aligia and J. Garcés, Phys. Rev. B **49**, 524 (1994).
[4] V. I. Kudinov, I. L. Chaplygin, A. I. Kirilyuk, N. M. Kreines, R. Laiho, E. Lähderanta, and C. Ayache, Phys. Rev. B **47**, 9017 (1993).
[5] G. Uimin, Phys. Rev. B **50**, 9531 (1994).
[6] V. I. Kudinov, A. I. Kirilyuk, N. M. Kreines, R. Laiho, and E. Lähderanta, Phys. Lett. A **151**, 358 (1990).
[7] G. Nieva, E. Osquiguil, J. Guimpel, M. Maenhoudt, B. Wuyts, Y. Bruynseraede, M. B. Maple, and I. K. Schuller, Appl. Phys. Lett. **60**, 2159 (1992).
[8] C. Thomsen, M. Cardona, B. Gegenheimer, R. Liu, and A. Simon, Phys. Rev. B **37**, 9860 (1988).
[9] D. R. Wake, F. Slakey, M. V. Klein, J. P. Rice, and D. M. Ginsberg, Phys. Rev. Lett. **67**, 3728 (1991).
[10] A. Fainstein, P. Etchegoin, and J. Guimpel, Phys. Rev. B **58**, 9433 (1998).
[11] M. Käll, M. Osada, M. Kakihana, L. Börjesson, T. Frello, J. Madsen, N. H. Andersen, R. Liang, P. Dosanjh, and W. N. Hardy, Phys. Rev. B **57**, R14 072 (1998).
[12] A. G. Panfilov, A. I. Rykov, S. Tajima, and A. Yamanaka, Phys. Rev. B **58**, 12 459 (1998).
[13] V. G. Ivanov, M. N. Iliev, and C. Thomsen, Phys. Rev. B **52**, 13 652 (1995).
[14] E. Osquiguil, M. Maenhoudt, B. Wuyts, Y. Bruynseraede, D. Lederman, and I. K. Schuller, Phys. Rev. B **49**, 3675 (1994).
[15] K. Kawamoto and I. Hirabayashi, Phys. Rev. B **49**, 3655 (1994).
[16] A. Fainstein, B. Maiorov, J. Guimpel, G. Nieva, and E. Osquiguil, Phys. Rev. B **61**, 4298 (2000).
[17] M. Guillaume, P. Allenspach, W. Henggeler, J. Mesot, B. Roessli, U. Staub, P. Fischer, A. Furrer, and V. Trounov, J. Phys.: Condens. Matter **6**, 7963 (1994).
[18] G. Nieva, S. Ghamaty, B. W. Lee, M. B. Maple, and I. K. Schuller, Phys. Rev. B **44**, 6999 (1991).
[19] E. Osquiguil, M. Maenhoudt, B. Wuyts, and Y. Bruynseraede, Appl. Phys. Lett. **60**, 1627 (1992).
[20] F. Prado, A. Caneiro, and A. Serquis, Physica C **295**, 235 (1998).
[21] T. B. Lindemer and E. D. Specht, Physica C **268**, 271 (1996).
[22] T. B. Lindemer, B. C. Chakoumakos, E. D. Specht, R. K. Williams, and Y. J. Chen, Physica C **231**, 80 (1994); E. Takayama-Muromachi, Y. Uchida, A. Fujimori, and K. Kato, Jpn. J. Appl. Phys., Part 2 **27**, L233 (1988).
[23] R. Liu, C. Thomsen, W. Kress, M. Cardona, B. Gegenheimer, F. W. de Wette, J. Prade, A. D. Kulkarni, and U. Schröder, Phys. Rev. B **37**, 7971 (1988).
[24] M. Cardona, R. Liu, C. Thomsen, M. Bauer, L. Genzel, W. König, A. Wittlin, U. Amador, M. Barahona, F. Fernandez, C. Otero, and R. Saez, Solid State Commun. **65**, 71 (1988).
[25] H. J. Rosen, R. M. Macfarlane, E. M. Engler, V. Y. Lee, and R. D. Jacowitz, Phys. Rev. B **38**, 2460 (1988).
[26] The notation for the atom positions in the unit cell is the same as in Ref. 23.
[27] A. G. Panfilov, M. F. Limonov, A. I. Rykov, S. Tajima, and A. Yamanaka, Phys. Rev. B **57**, R5634 (1998).
[28] See, e.g., J. Kakalios, R. A. Street, and W. B. Jackson, Phys. Rev. Lett. **59**, 1037 (1987).
[29] H. Scher, M. F. Shlesinger, and J. T. Bendler, Phys. Today **44** (1), 26 (1991); M. F. Shlesinger, Annu. Rev. Phys. Chem. **39**, 269 (1988).
[30] C. Ambrosch-Draxl, P. A. Korzhavyi, and B. Johansson, Physica C **341–348**, 1997 (2000).
[31] P. Nagel, V. Pasler, C. Meingast, A. I. Rykov, and S. Tajima, Phys. Rev. Lett. **85**, 2376 (2000).
[32] W. Kress, U. Schröder, J. Prade, A. D. Kulkarni, and F. W. de Wette, Phys. Rev. B **38**, 2906 (1988).